New Sliding-Mode Observer for Position Sensorless Control of Permanent-Magnet Synchronous Motor

Zhaowei Qiao, Tingna Shi, Yindong Wang, Yan Yan, Changliang Xia, *Senior Member, IEEE*, and Xiangning He, *Fellow, IEEE*

***Abstract*—This paper proposes a novel sliding-mode observer (SMO) to achieve the sensorless control of permanent-magnet synchronous motor (PMSM). An observer is built according to the back electromotive force (EMF) model after the back EMF equivalent signal is obtained. In this way, not only are low-pass filter and phase compensation module eliminated, but also estimation accuracy is improved. Numerical simulations and experiments with an 11-kW low-speed PMSM are carried out. The results demonstrate that the novel SMO can effectively estimate rotor position and speed and achieve good static and dynamic performance.**

***Index Terms*—Back electromotive force (EMF), permanent-magnet synchronous motor (PMSM), sensorless, sliding-mode observer (SMO).**

I. Introduction

PERMANENT-MAGNET synchronous motor (PMSM) has been widely used in various fields due to its high power density, high efficiency, and simple structure. As an important application of PMSM, the motion control requires not only the accurate knowledge of rotor position for field orientation but also the information of rotor speed for closed-loop control; thus, position transducers such as an optical encoder and a resolver are needed to be installed on the shaft [1], [2]. However, the installation of a position transducer will result in greater cost and bigger size of drives and limit the application of PMSM in a relatively harsh environment [3]. Nowadays, digital signal processors (DSPs) have become more attractive as they allow the implementation of complex control strategies [4]–[10], which made the sensorless control technique of PMSM become possible.

Currently, the sensorless control technology can mainly be classified into two types: the estimation method based on observer [11]–[18] and the high-frequency injection method using the salient effect of motor [19]–[24]. Model reference adaptive method [13]–[15] and extended Kalman filtering method [16]–[18] belong to the scope of method based on observer. The estimation method based on observer relies on the accuracy of the motor model to some extent, which affects the estimation performance. In [25], online parameter identification is adopted to improve the accuracy of the position estimation. The high-frequency injection method is independent of the motor model, but the high-frequency injection signal will bring high-frequency noise which leads to system performance degradation. Given the aforementioned circumstances, the sliding-mode observer (SMO) is widely used because of its simple algorithm and robustness, which makes up for the dependence of the observer on the model to a certain extent [26]–[31].

The SMO maintains good robustness of variable structure control [32]–[34]. The control loop in an ordinary observer is replaced by a sliding-mode variable structure [35], [36], and when the system error reaches the sliding mode, the system dynamic performance entirely depends on the sliding surface, which ensures good robustness of the entire system to parameter variations [37], [38]. Due to the discrete switch control in the SMO, chattering becomes the inherent characteristic of the sliding-mode variable structure system. As chattering cannot be completely eliminated but only reduced, in the design of the system, there should be a tradeoff between chattering reduction and system robustness. For the traditional SMO, the switch function is used as the control function. Due to switch time and space lag, the SMO presents serious chattering [39], [40]. The estimated signal of the SMO contains high-frequency oscillation components, so one or several low-pass filters are usually used to extract the required back electromotive force (EMF) signal. However, the introduction of low-pass filters usually causes phase delay, which should be compensated for according to the actual angular frequency. Thus, this cannot meet the control requirements of high-performance applications. In [41], an adaptive filter is proposed, which still fails to completely compensate for phase delay. In [42], two cascaded SMOs are used, but multiple low-pass filters increase the phase delay.

To solve the aforementioned problems, a new SMO is proposed to achieve the sensorless control of PMSM. Its advantages can be listed as follows. The conventional switch function is replaced by the sigmoid function to reduce system chattering; an observer is constructed according to the back EMF model to extract the back EMF signal, thus improving the effect of estimation.

Manuscript received June 13, 2012; accepted June 14, 2012. Date of publication July 6, 2012; date of current version September 13, 2012. This work was supported in part by the Key Program of National Natural Science Foundation of China under Grant 51037004, by the National Natural Science Foundation of China under Grant 51077097, and by the Key Technologies Research and Development Program of Tianjin under Grant 11ZCKFGX03300.

Z. Qiao, T. Shi, and Y. Yan are with the School of Electrical Engineering and Automation, Tianjin University, Tianjin 300072, China (e-mail: zwqiao@tju.edu.cn; tnshi@tju.edu.cn; yanyan@tju.edu.cn).

Y. Wang is with Aviation Industry Corporation of China Tianjin Aviation Electro-Mechanical Company, Ltd., Tianjin 300308, China (e-mail: yindong@tju.edu.cn).

C. Xia is with the School of Electrical Engineering and Automation, Tianjin University, Tianjin 300072, China, and also with the Tianjin Key Laboratory of Advanced Technology of Electrical Engineering and Energy, Tianjin Polytechnic University, Tianjin 300387, China (e-mail: motor@tju.edu.cn).

X. He is with the College of Electrical Engineering, Zhejiang University, Hangzhou 310027, China (e-mail: hxn@zju.edu.cn).

Digital Object Identifier 10.1109/TIE.2012.2206359

II. Mathematical Model of PMSM

The PMSM model in the stationary reference frame (α, β) is shown as follows:

$$\begin{cases} L_s\left(\frac{di_\alpha}{dt}\right) = -R_s i_\alpha - e_\alpha + u_\alpha \\ L_s\left(\frac{di_\beta}{dt}\right) = -R_s i_\beta - e_\beta + u_\beta \\ e_\alpha = -\psi_f \omega_r \sin\theta \\ e_\beta = \psi_f \omega_r \cos\theta \end{cases} \tag{1}$$

where i_α, i_β, u_α, u_β, and e_α, e_β are the phase currents, phase voltages, and back EMF in the stationary reference frame, respectively, R_s is the stator phase resistance, L_s is the stator phase inductance, ψ_f is the flux linkage of the permanent magnet, ω_r is the electrical angular velocity, and θ is the electrical rotor position.

It can be seen from the back EMF function in (1) that the back EMF signal contains the information of rotor speed and position. Therefore, after the back EMF signal is estimated by using the observer, the information of rotor speed and position can be obtained.

III. Design of SMO

A. Improved Current Observer

Based on the sliding-mode variable structure theory, the sliding surface is selected as

$$\boldsymbol{S}(X) = \hat{\boldsymbol{i}}_s - \boldsymbol{i}_s = \boldsymbol{0} \tag{2}$$

where $\hat{\boldsymbol{i}}_s = [\hat{i}_\alpha \ \hat{i}_\beta]^{\mathrm{T}}$ is the estimated current value and $\boldsymbol{i}_s = [i_\alpha \ i_\beta]^{\mathrm{T}}$ is the actual measure value.

By using the mathematical model of PMSM in the stationary (α, β) reference frame, the SMO is shown as follows:

$$\begin{cases} L_s\left(\frac{d\hat{i}_\alpha}{dt}\right) = -R_s\hat{i}_\alpha + u_\alpha - k\mathrm{sgn}(\hat{i}_\alpha - i_\alpha) \\ L_s\left(\frac{d\hat{i}_\beta}{dt}\right) = -R_s\hat{i}_\beta + u_\beta - k\mathrm{sgn}(\hat{i}_\beta - i_\beta) \end{cases} \tag{3}$$

where k is a constant observer gain, $\mathrm{sgn}(x)$ is the sign function, and (3) is the conventional SMO. In order to reduce the chattering phenomenon, the sign function is replaced by a continuous function, i.e., the sigmoid function, which is defined as

$$F(x) = \left[\frac{2}{(1+e^{-ax})}\right] - 1 \tag{4}$$

where a is the adjustable parameter. Then, the SMO can be rewritten as

$$\begin{cases} L_s\left(\frac{d\hat{i}_\alpha}{dt}\right) = -R_s\hat{i}_\alpha + u_\alpha - kF(\hat{i}_\alpha - i_\alpha) \\ L_s\left(\frac{d\hat{i}_\beta}{dt}\right) = -R_s\hat{i}_\beta + u_\beta - kF(\hat{i}_\beta - i_\beta). \end{cases} \tag{5}$$

In order to verify the stability of the aforementioned SMO, the Lyapunov function is selected as

$$\boldsymbol{V} = \frac{1}{2}\boldsymbol{S}(X)^{\mathrm{T}}\boldsymbol{S}(X). \tag{6}$$

The stability condition of the SMO is as follows:

$$\dot{\boldsymbol{V}} = \boldsymbol{S}(X)^{\mathrm{T}}\dot{\boldsymbol{S}}(X) \le 0. \tag{7}$$

The error equation is obtained by subtracting (1) from (5) as

$$\begin{cases} L_s\left[\frac{dS_\alpha(X)}{dt}\right] = -R_s S_\alpha(X) + e_\alpha - kF(\hat{i}_\alpha - i_\alpha) \\ L_s\left[\frac{dS_\beta(X)}{dt}\right] = -R_s S_\beta(X) + e_\beta - kF(\hat{i}_\beta - i_\beta) \end{cases} \tag{8}$$

where

$$\boldsymbol{S}(X) = \begin{bmatrix} S_\alpha(X) \\ S_\beta(X) \end{bmatrix} = \begin{bmatrix} \hat{i}_\alpha - i_\alpha \\ \hat{i}_\beta - i_\beta \end{bmatrix}.$$

Through the above derivation, the stability condition can be expressed as

$$\begin{aligned} \dot{\boldsymbol{V}} &= \boldsymbol{S}(X)^{\mathrm{T}}\dot{\boldsymbol{S}}(X) = \boldsymbol{S}_\alpha\dot{\boldsymbol{S}}_\alpha + \boldsymbol{S}_\beta\dot{\boldsymbol{S}}_\beta \\ &= \frac{1}{L_s}\left[(\hat{i}_\alpha - i_\alpha)e_\alpha - k(\hat{i}_\alpha - i_\alpha)F(\hat{i}_\alpha - i_\alpha)\right] \\ &\quad + \frac{1}{L_s}\left[(\hat{i}_\beta - i_\beta)e_\beta - k(\hat{i}_\beta - i_\beta)F(\hat{i}_\beta - i_\beta)\right] \\ &\quad - \frac{R_s}{L_s}\left[(\hat{i}_\alpha - i_\alpha)^2 + (\hat{i}_\beta - i_\beta)^2\right] \le 0. \end{aligned}$$

As a result

$$k > \max\left(|e_\alpha||e_\beta|\right). \tag{9}$$

Therefore, k, which is large enough, can ensure both the existence of sliding motion and the asymptotical stability of sliding motion in the global scope. Once the system reaches the sliding surface, then

$$\dot{\boldsymbol{S}}(X) = \boldsymbol{S}(X) = \boldsymbol{0}. \tag{10}$$

Based on the equivalent control method, substituting the above equation into (8) yields

$$\begin{aligned} e_\alpha &= kF(\hat{i}_\alpha - i_\alpha) \\ e_\beta &= kF(\hat{i}_\beta - i_\beta). \end{aligned} \tag{11}$$

B. Rotor Position and Speed Estimate

The equivalent back EMF can be obtained through the aforementioned SMO, but the signal still contains high-frequency components and cannot be directly used to calculate rotor position and speed. In the traditional SMO, a first-order low-pass filter is commonly used for filtering, thus causing phase delay which is related to its own cutoff frequency and the angular frequency of the input signal. To completely compensate for the phase delay, the real-time angular velocity information must be used, and due to the estimated value of angular velocity, the effect of compensation will be affected. Therefore, in order to avoid the use of the low-pass filter and phase compensation part,

based on the back EMF model, this paper constructs an observer to extract the back EMF signal so as to estimate rotor position and speed.

Because the change rate of motor angular velocity is far less than that of stator current, assuming $\dot{\omega}_r = 0$, then the back EMF model of PMSM can be expressed as

$$\begin{aligned} \frac{de_\alpha}{dt} &= -\omega_r e_\beta \\ \frac{de_\beta}{dt} &= \omega_r e_\alpha. \end{aligned} \tag{12}$$

Based on the above equations, a back EMF observer is constructed

$$\begin{cases} \frac{d\hat{e}_\alpha}{dt} = -\hat{\omega}_r \hat{e}_\beta - l(\hat{e}_\alpha - e_\alpha) \\ \frac{d\hat{e}_\beta}{dt} = \hat{\omega}_r \hat{e}_\alpha - l(\hat{e}_\beta - e_\beta) \\ \frac{d\hat{\omega}_r}{dt} = (\hat{e}_\alpha - e_\alpha)\hat{e}_\beta - (\hat{e}_\beta - e_\beta)\hat{e}_\alpha \end{cases} \tag{13}$$

where l is the observer gain, whose value is greater than zero.

By subtracting (12) from (13) and doing further consolidation, the error equation of the observer is obtained as

$$\begin{cases} \frac{d\tilde{e}_\alpha}{dt} = -\tilde{\omega}_r \hat{e}_\beta - \omega_r \tilde{e}_\beta - l\tilde{e}_\alpha \\ \frac{d\tilde{e}_\beta}{dt} = \tilde{\omega}_r \hat{e}_\alpha + \omega_r \tilde{e}_\alpha - l\tilde{e}_\beta \\ \frac{d\tilde{\omega}_r}{dt} = \tilde{e}_\alpha \hat{e}_\beta - \tilde{e}_\beta \hat{e}_\alpha \end{cases} \tag{14}$$

where $\tilde{e}_\alpha = \hat{e}_\alpha - e_\alpha$, $\tilde{e}_\beta = \hat{e}_\beta - e_\beta$, and $\tilde{\omega}_r = \hat{\omega}_r - \omega_r$.

To prove the stability of (13), the Lyapunov function is defined as

$$\boldsymbol{V} = \frac{\left(\tilde{e}_\alpha^2 + \tilde{e}_\beta^2 + \tilde{\omega}_r^2\right)}{2}. \tag{15}$$

Differentiating the above equation yields

$$\dot{\boldsymbol{V}} = \tilde{e}_\alpha \dot{\tilde{e}}_\alpha + \tilde{e}_\beta \dot{\tilde{e}}_\beta + \tilde{\omega}_r \dot{\tilde{\omega}}_r. \tag{16}$$

Substituting (14) into the above equation yields

$$\dot{\boldsymbol{V}} = -l\left(\tilde{e}_\alpha^2 + \tilde{e}_\beta^2\right) \le 0. \tag{17}$$

It can be seen from the above equation that the back EMF observer is asymptotically stable. Therefore, by using the back EMF signal obtained from the observer and the relationship between the back EMF and the rotor position, the position signal is estimated as

$$\hat{\theta} = -\arctan\left(\frac{\hat{e}_\alpha}{\hat{e}_\beta}\right). \tag{18}$$

Moreover, the estimated value of speed can be directly obtained by integral operation in the observer.

According to the analysis of the aspects mentioned earlier, the control diagram of the sensorless control of PMSM is shown in Fig. 1, among which Fig. 1(a) is the overall block diagram and Fig. 1(b) is the structure diagram of the new SMO. In Fig. 1, it should be noted that the input of the SMO is the given motor voltage, which is restored by using the actual measurement of dc bus voltage and the duty cycle calculated from the space vector modulation module, whereas the given voltages of the current loop output u_α^* and u_β^* are not used. The use of u_α and u_β can partially eliminate the dead time effect of the inverter; thus, more accurate actual given motor voltage can be obtained to further improve the estimation accuracy of rotor position and speed.

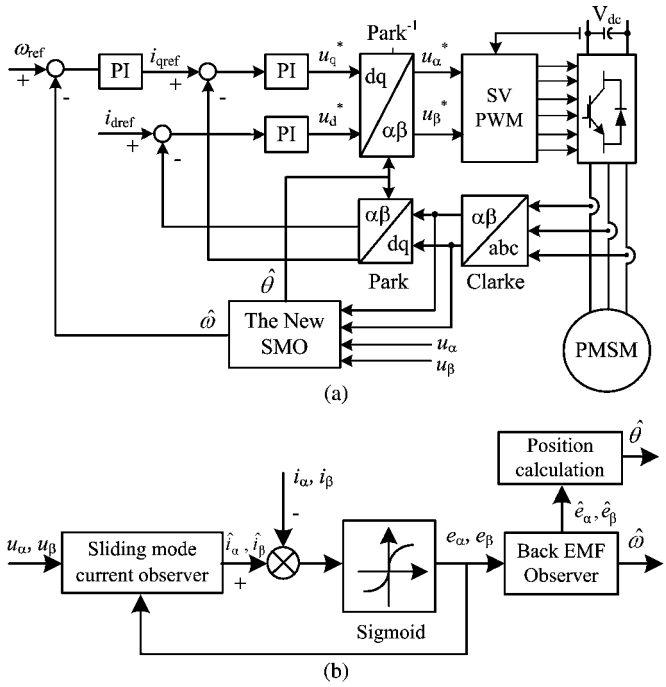

Fig. 1. Block diagram of sensorless vector control of PMSM. (a) Overall block diagram of the proposed system. (b) Block diagram of the new SMO.

TABLE I
PARAMETERS OF THE MOTOR

Parameters	Units	Values
Rated voltage U_N	V	380
Rated power P	kW	11
Rated speed n_N	r/min	150
Rotational inertia J	kg·m^2	3.74
Flux of permanent magnet φ_f	Wb	1.437
Stator resistance R_s	Ω	1.25
Stator inductance L_s	mH	12.5
Pole pairs p		12

IV. Simulation and Experimental Results

A. Simulation Results

In order to verify the validity of the new SMO, the proposed system from Fig. 1 has been implemented in the Matlab/Simulink programming environment. The $i_d = 0$ control mode is carried out on a PMSM with the parameters listed in Table I.

Figs. 2–4 show the three sets of simulation waveforms when the reference speed is a step signal. In the simulation, the reference speed is changed from 15 to 100 r/min, and the load torque is 100 N · m.

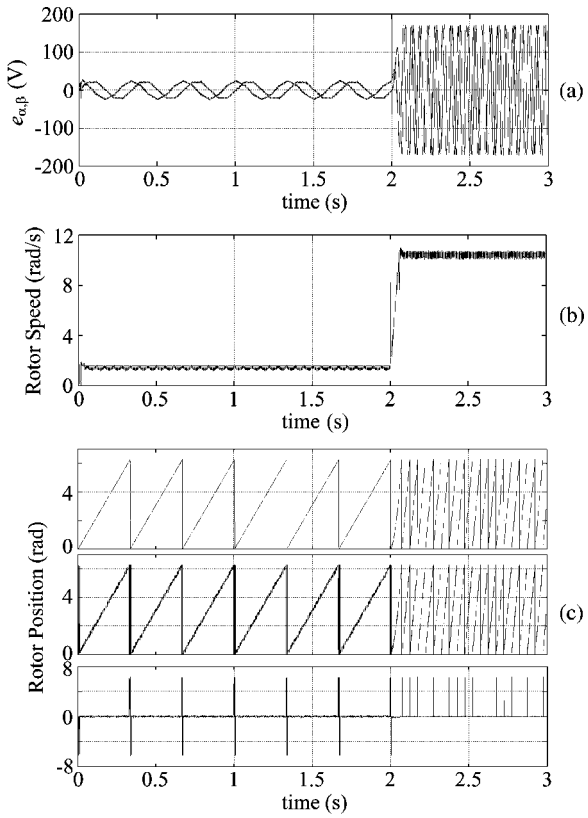

Fig. 2. Simulation waveforms obtained by the conventional method using sign function. (a) Estimated back EMF. (b) Actual and estimated speeds. (c) Actual rotor position, estimated rotor position, and estimated error.

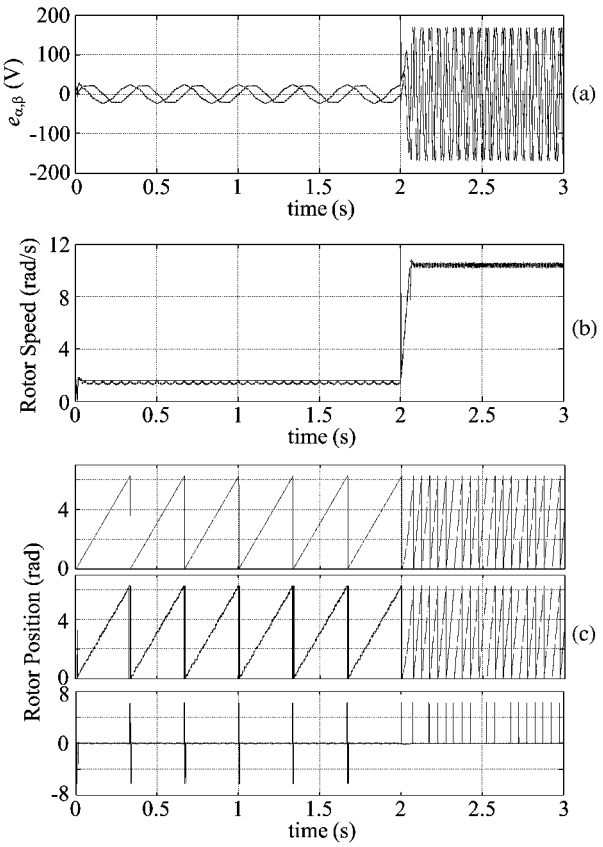

Fig. 3. Simulation waveforms obtained by the conventional method using a sigmoid function. (a) Estimated back EMF. (b) Actual and estimated speeds. (c) Actual rotor position, estimated rotor position, and estimated error.

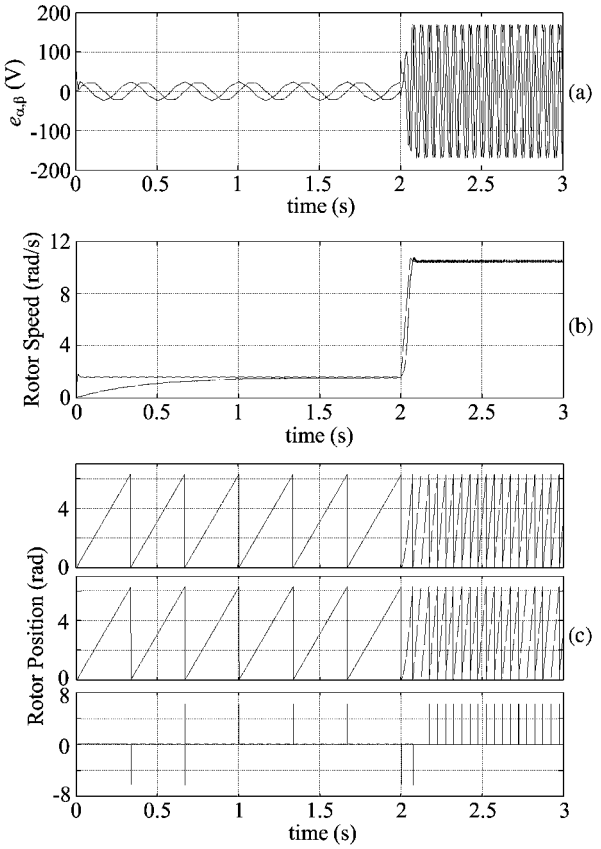

Fig. 4. Simulation waveforms obtained by the new SMO. (a) Estimated back EMF. (b) Actual and estimated speeds. (c) Actual rotor position, estimated rotor position, and estimated error.

Fig. 2 displays the simulation waveform obtained by the conventional method using a sign function. Fig. 3 gives the waveform obtained by the conventional method using a sigmoid function. Fig. 4 shows the simulation waveform obtained by the method proposed in this paper.

It can be seen from Figs. 2 and 3 that the chattering phenomenon is reduced when the sign function is replaced by a sigmoid function. However, both methods still use the low-pass filter and phase compensation part, and therefore, the rotor position estimation accuracy is not high. It can be seen from Fig. 4 that the chattering phenomenon of the estimated rotor position and speed is reduced, and the accuracy of rotor position estimation is improved to some extent.

Fig. 5 shows the estimation performance of the proposed method when the parameters of PMSM vary. In the simulation, the reference speed is 30 r/min, and the load torque is 100 N · m.

It can be seen from Fig. 5 that, when the resistance or the inductance of the motor changes, the estimated speed can still converge to the actual value, which verifies the robustness of the proposed approach.

Figs. 6 and 7 show the simulation waveforms when the parameter l in the back EMF observer is set as different values. In the simulation, the reference speed steps up from 15 to 100 r/min, and the load torque is 100 N · m.

As can be seen from Fig. 7, the variation of l has little effect on the estimation of rotor position, and when l increases, the convergence rate of the estimated speed declines.

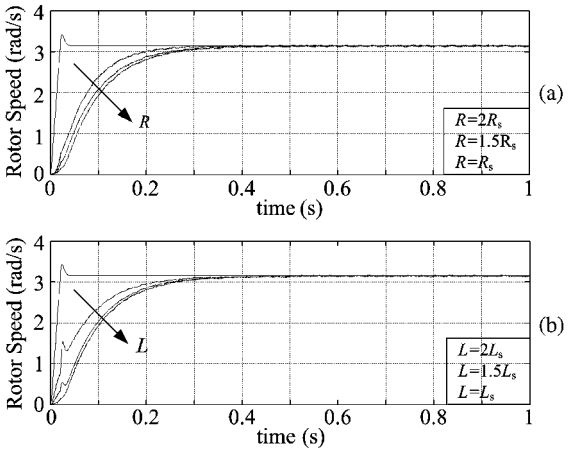

Fig. 5. Simulation waveforms when the parameters of PMSM are changed. (a) Waveforms when the resistance is changed. (b) Waveforms when the inductance is changed.

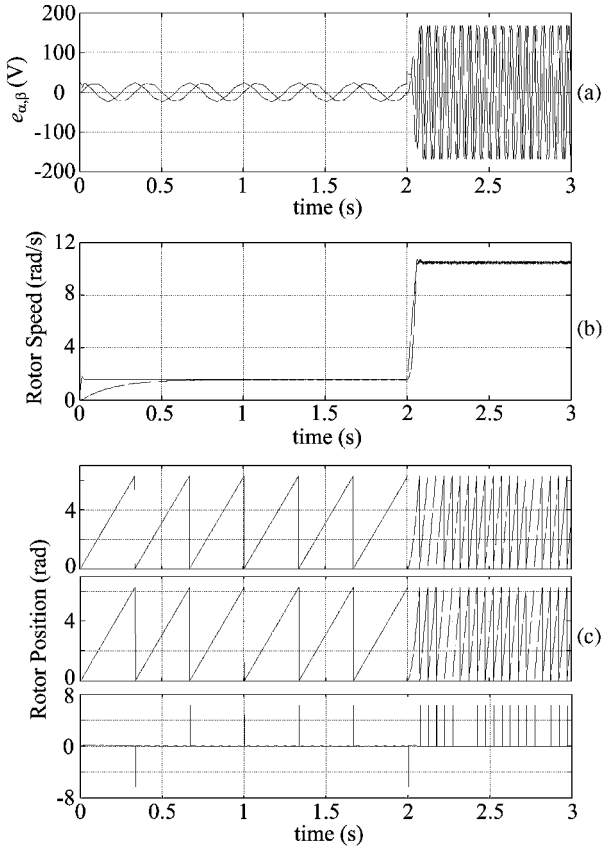

Fig. 6. Simulation waveforms when $l = 100$. (a) Estimated back EMF. (b) Actual and estimated speeds. (c) Actual rotor position, estimated rotor position, and estimated error.

Fig. 8 shows the simulation waveforms when the motor is in positive and negative revolution. In the simulation, the reference speed is changed from $+15$ to -15 r/min, and the load torque is 100 N $\cdot$ m. As can be seen from Fig. 8, when the reference speed is changed from $+15$ to -15 r/min, the new SMO can effectively obtain the estimated rotor position and speed.

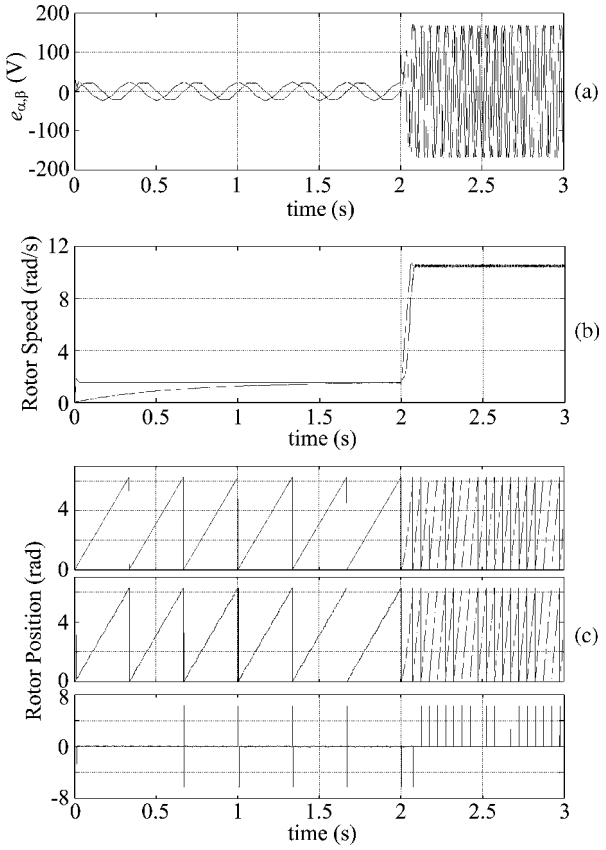

Fig. 7. Simulation waveforms when $l = 300$. (a) Estimated back EMF. (b) Actual and estimated speeds. (c) Actual rotor position, estimated rotor position, and estimated error.

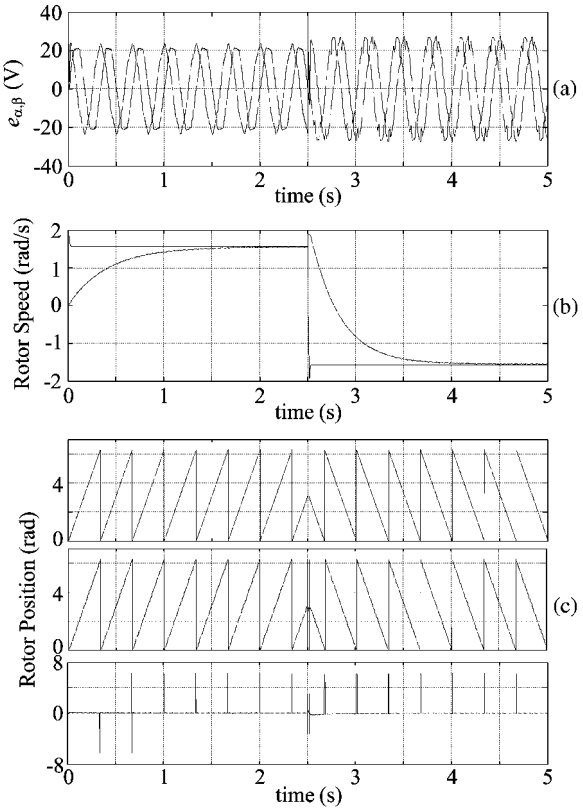

Fig. 8. Simulation waveforms when the reference speed is changed from $+15$ to -15 r/min. (a) Estimated back EMF. (b) Actual and estimated speeds. (c) Actual rotor position, estimated rotor position, and estimated error.

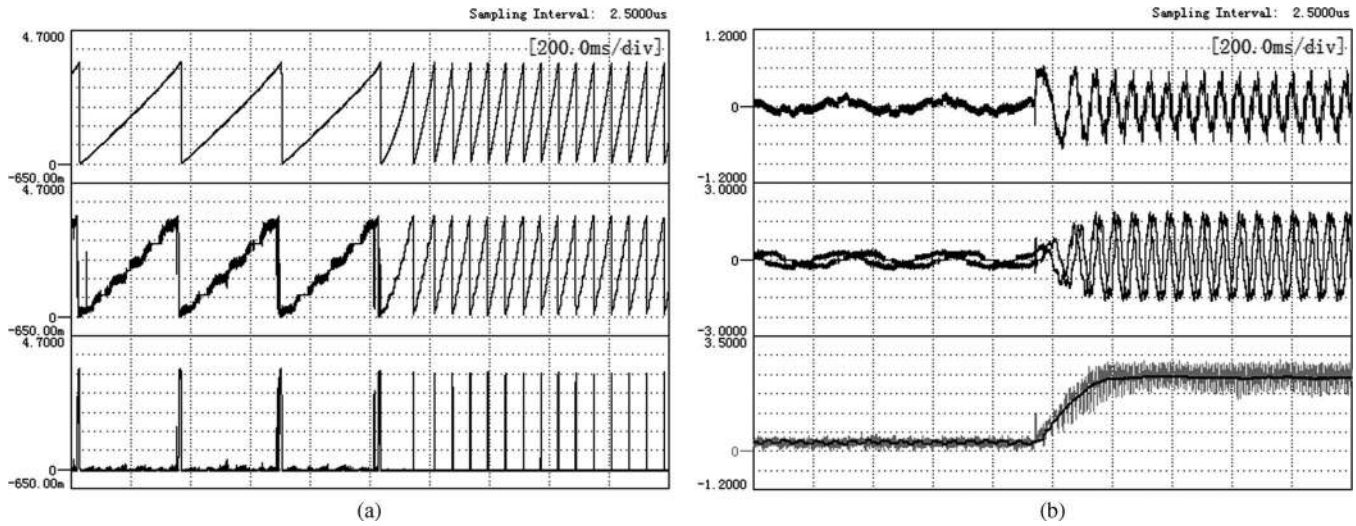

Fig. 9. Operating waveforms obtained by the conventional method using the sign function. (a) From top to bottom are the actual rotor position, estimated rotor position, and estimated error (67.8 °/div), respectively. (b) From top to bottom are the A-phase stator current (4.5 A/div), the estimated back EMF (85 V/div), and the actual and the estimated speed (30 r/min/div), respectively.

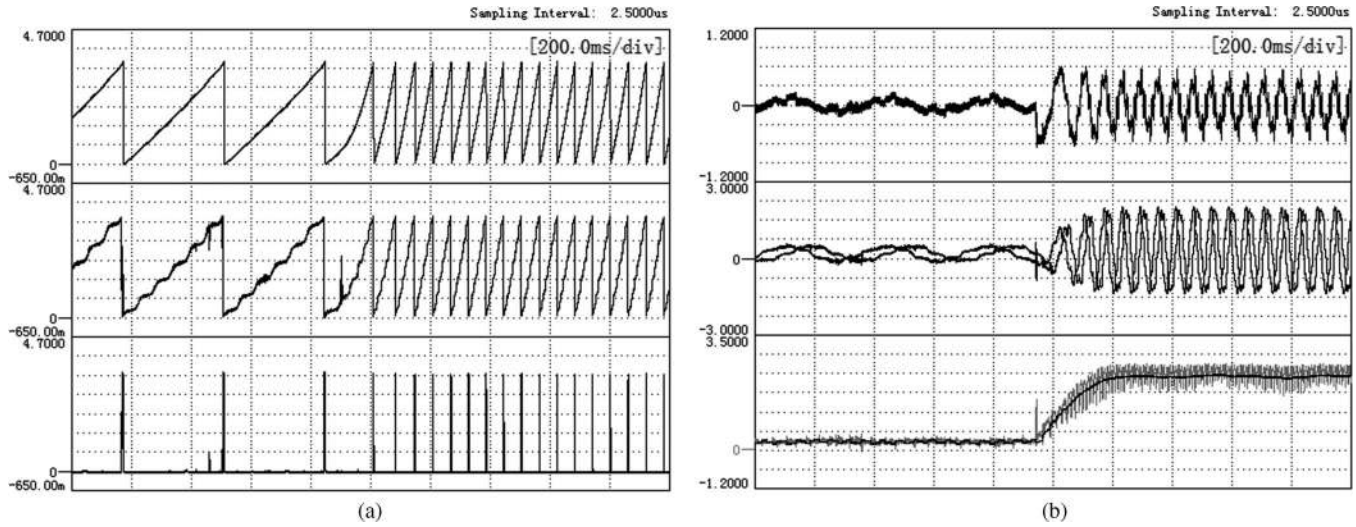

Fig. 10. Operating waveforms obtained by the conventional method using a sigmoid function. (a) From top to bottom are the actual rotor position, estimated rotor position, and estimated error (67.8 °/div), respectively. (b) From top to bottom are the A-phase stator current (4.5 A/div), the estimated back EMF (85 V/div), and the actual and the estimated speed (30 r/min/div), respectively.

B. Experimental Results

To further verify the performance of the new SMO for estimating rotor position and speed, in this paper, the vector control platform of PMSM based on a SMO is constructed by using a set of PMSM and generator. A floating-point TMS320F28335 DSP is employed as the digital controller, the space vector modulation algorithm is used as modulation strategy, the switching frequency is 5 kHz, and the sampling period of the control system is set as 120 μs. The motor parameters are given in Table I.

1) Comparison Between the Traditional Method and the Proposed Method: Figs. 9–11 show the waveforms when the PMSM is running with load and the reference speed steps up from 15 to 100 r/min. Fig. 9 shows the waveforms when the conventional method based on the sign function and low-pass filter is adopted.

As can be seen from Fig. 9, due to the use of the sign function, the chattering of the estimated rotor position and speed obtained by the traditional method is significant.

Fig. 10 shows the waveforms when the method based on the sigmoid function and low-pass filter is used, and Fig. 11 shows the waveforms when the new SMO is adopted. It can be seen from Fig. 10 that the chattering is reduced when the sign function is replaced by the sigmoid function, but the chattering of the estimated speed cannot be neglected when the PMSM is running at 100 r/min. As can be seen from Fig. 11, compared with the aforementioned two methods, the waveforms of the estimated rotor position and speed obtained by the new SMO are smooth, and the chattering is reduced. In addition, the estimated back EMF waveforms obtained by the three methods are not the ideal sinusoidal waveform, which is due to the design of the motor itself.

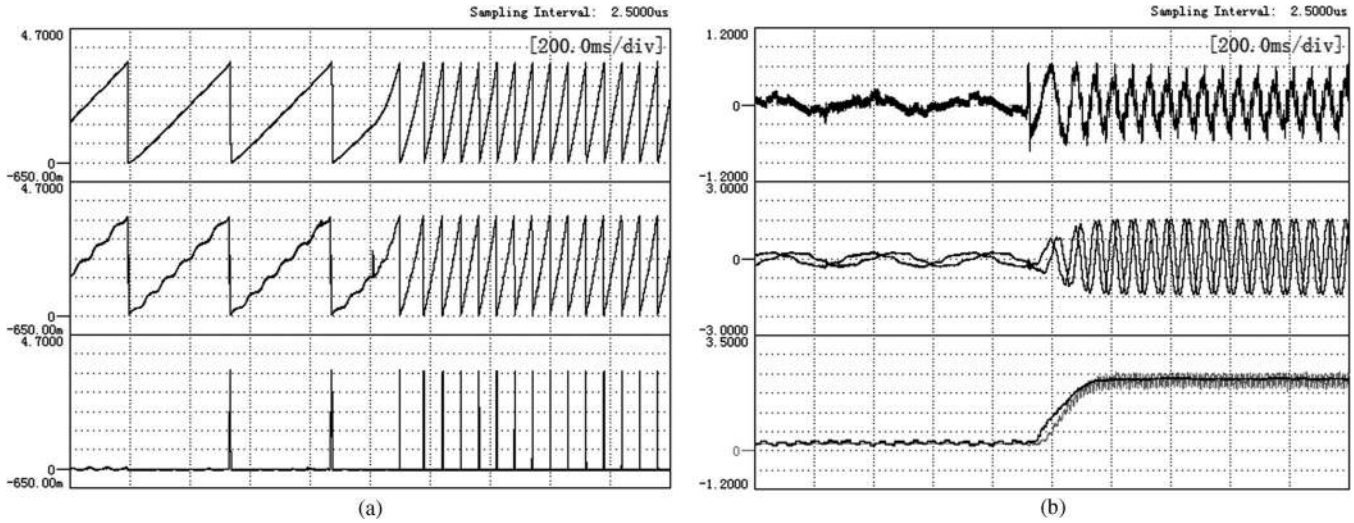

Fig. 11. Operating waveforms obtained by the new SMO. (a) From top to bottom are the actual rotor position, estimated rotor position, and estimated error (67.8 °/div), respectively. (b) From top to bottom are the A-phase stator current (4.5 A/div), the estimated back EMF (85 V/div), and the actual and the estimated speed (30 r/min/div), respectively.

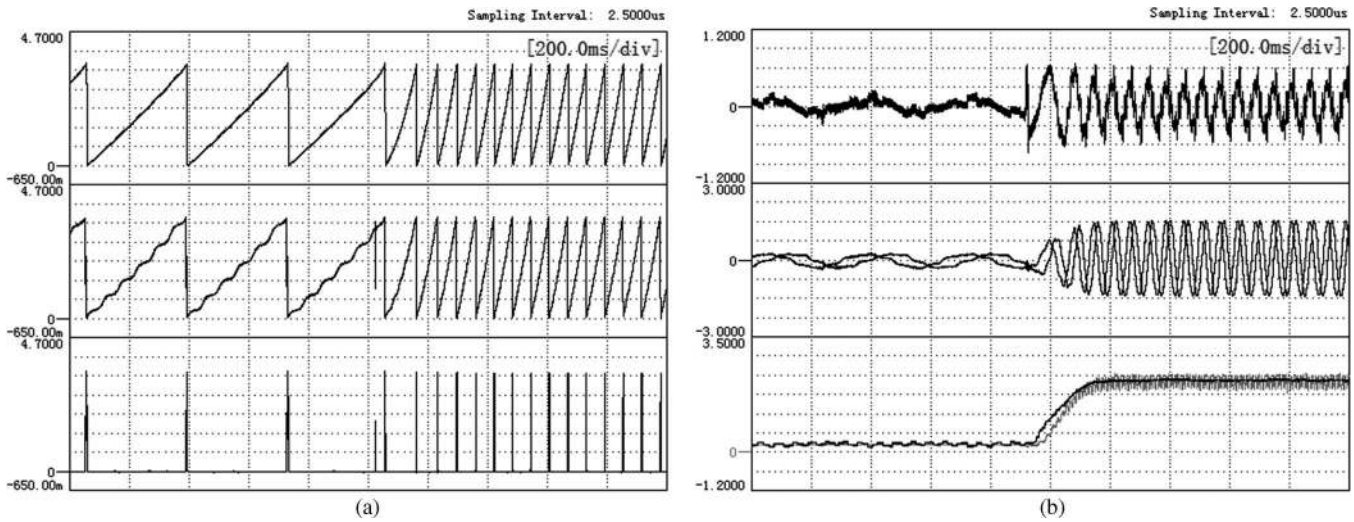

Fig. 12. Operating waveforms when resistors are in series with the three-phase stator windings. (a) From top to bottom are the actual rotor position, estimated rotor position, and estimated error (67.8 °/div), respectively. (b) From top to bottom are the A-phase stator current (4.5 A/div), the estimated back EMF (85 V/div), and the actual and the estimated speed (30 r/min/div), respectively.

2) Performance of the New SMO With Changing Parameters: In order to discuss the performance of the new SMO, the related experiments with changing parameters are conducted. Fig. 12 shows the waveforms when some 2-Ω resistors are connected in series with the three-phase stator windings, the reference speed steps up from 15 to 100 r/min, and the PMSM is running with load.

It can be seen from Fig. 12 that, when the parameters of the motor are changed, the new SMO is still able to obtain the estimated rotor position and speed accurately. Therefore, the robustness of the proposed method can be proved.

Figs. 13 and 14 show the experimental waveforms when l is set to be different values. The reference speed steps up from 15 to 100 r/min, and the PMSM is running with load. It can be seen from the aforementioned two sets of waveforms that the estimated rotor position is not greatly affected when l changes, but the convergence rate of the estimated speed is reduced when l becomes larger.

3) Performance of the New SMO in Positive and Negative Revolution: To further verify the performance of the new SMO, the positive and negative revolution experiment is carried out. Fig. 15 shows the experimental waveforms, where the reference speed is changed from $+15$ to -15 r/min and the PMSM is running with load.

It can be seen from Fig. 15 that, when the reference speed is changed from $+15$ to -15 r/min, the estimated rotor position and speed obtained by the new SMO can accurately converge to their actual values.

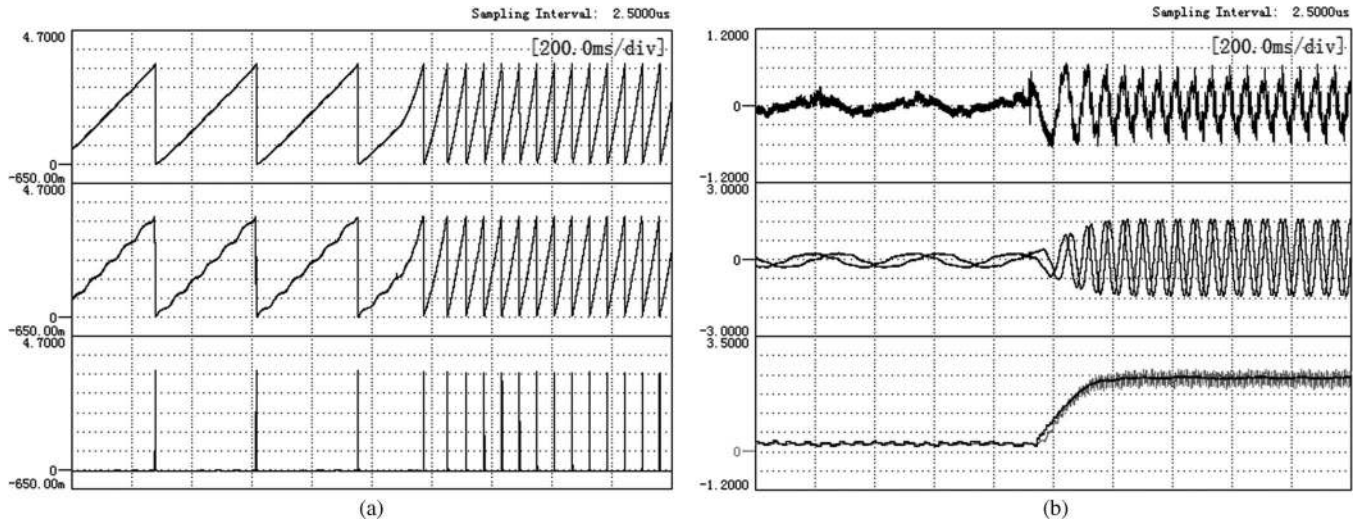

Fig. 13. Operating waveforms when $l = 100$. (a) From top to bottom are the actual rotor position, estimated rotor position, and estimated error (67.8 °/div), respectively. (b) From top to bottom are the A-phase stator current (4.5 A/div), the estimated back EMF (85 V/div), and the actual and the estimated speed (30 r/min/div), respectively.

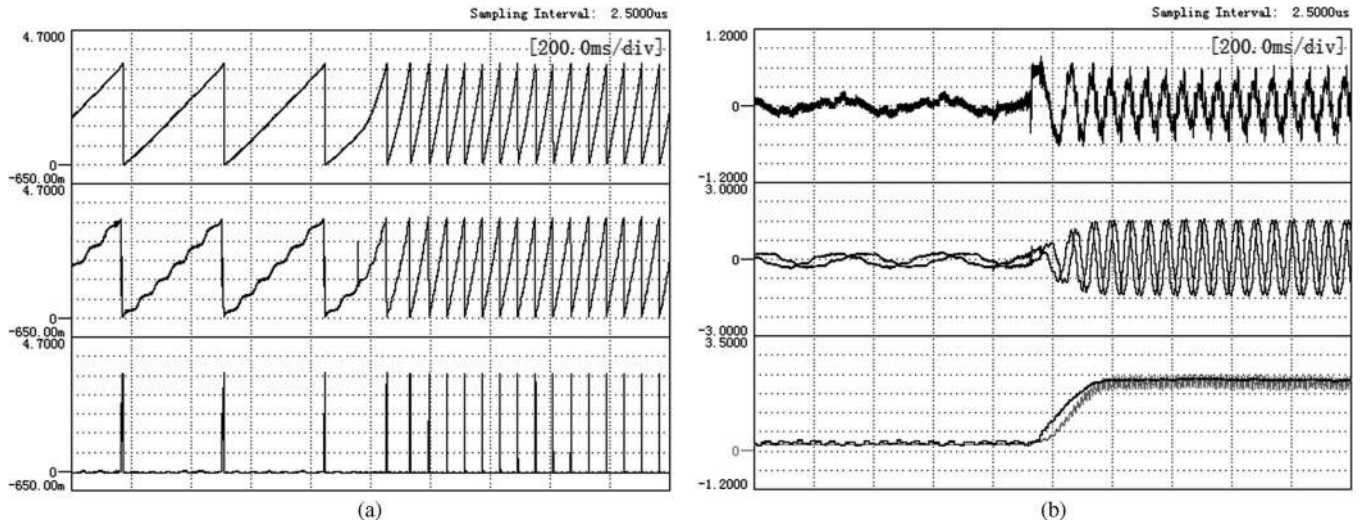

Fig. 14. Operating waveforms when $l = 300$. (a) From top to bottom are the actual rotor position, estimated rotor position, and estimated error (67.8 °/div), respectively. (b) From top to bottom are the A-phase stator current (4.5 A/div), the estimated back EMF (85 V/div), and the actual and the estimated speed (30 r/min/div), respectively.

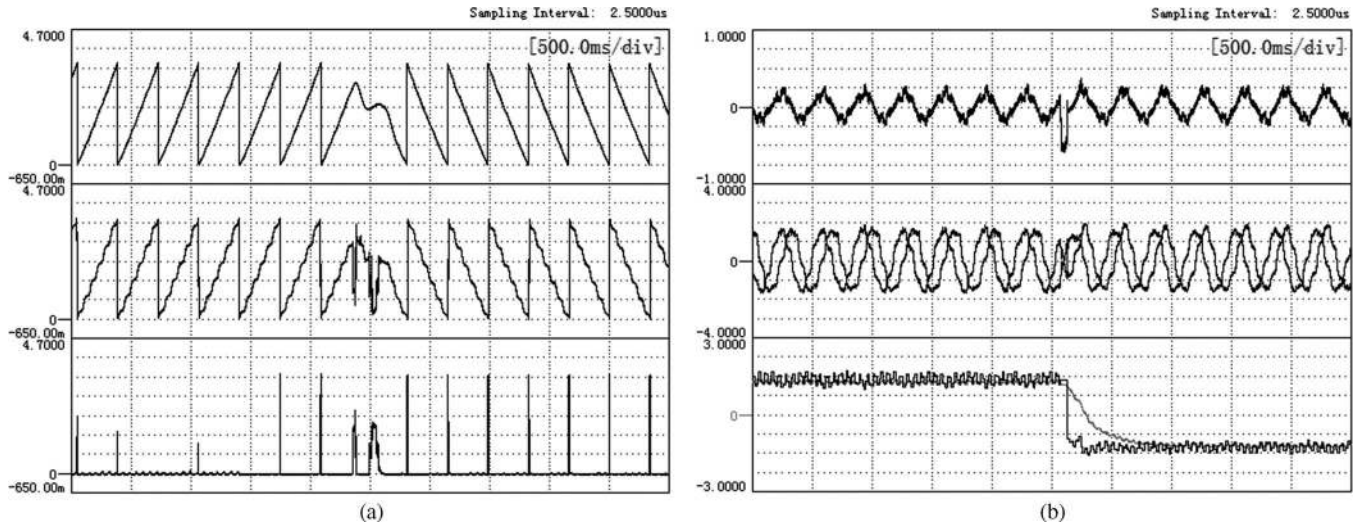

Fig. 15. Operating waveforms when the reference speed is changed from +15 to −15 r/min. (a) From top to bottom are the actual rotor position, estimated rotor position, and estimated error (67.8 °/div), respectively. (b) From top to bottom are the A-phase stator current (3.8 A/div), the estimated back EMF (13 V/div), and the actual and the estimated speed (8.5 r/min/div), respectively.

V. Conclusion

In this paper, the SMO is used to estimate the rotor position and speed of the PMSM due to its strong robustness, the sign function is replaced by the sigmoid function to reduce system chattering, and the traditional SMO is improved. The back EMF observer is constructed to extract the back EMF signal, which improves the estimation accuracy of rotor position and speed. Simulation and experimental results validate the feasibility and effectiveness of the new SMO for estimating the rotor position and speed of the PMSM. Compared with the traditional SMO, the new SMO has not only relatively simple structure but also better estimation performance.

References

[1] H. Liu and S. Li, "Speed control for PMSM servo system using predictive functional control and extended state observer," *IEEE Trans. Ind. Electron.*, vol. 59, no. 2, pp. 1171–1183, Feb. 2012.

[2] B. Alecsa, M. N. Cirstea, and A. Onea, "Simulink modeling and design of an efficient hardware-constrained FPGA-based PMSM speed controller," *IEEE Trans. Ind. Informat.*, vol. 8, no. 3, pp. 554–562, Aug. 2012.

[3] M. Pacas, "Sensorless drives in industrial applications," *IEEE Ind. Electron. Mag.*, vol. 5, no. 2, pp. 16–23, Jun. 2011.

[4] C. Buccella, C. Cecati, and H. Latafat, "Digital control of power converters—A survey," *IEEE Trans. Ind. Informat.*, vol. 8, no. 3, pp. 437–447, Aug. 2012.

[5] T. Atalik, M. Deniz, E. Koc, C. Gercek, B. Gultekin, M. Ermis, and I. Cadirci, "Multi-DSP and -FPGA based fully-digital control system for cascaded multilevel converters used in FACTS applications," *IEEE Trans. Ind. Informat.*, vol. 8, no. 3, pp. 511–527, Aug. 2012.

[6] A. Al Nabulsi and R. Dhaouadi, "Efficiency optimization of a DSP-based standalone PV system using fuzzy logic and dual-MPPT control," *IEEE Trans. Ind. Informat.*, vol. 8, no. 3, pp. 573–584, Aug. 2012.

[7] M. Rivera, J. Rodriguez, J. R. Espinoza, and H. Abu-Rub, "Instantaneous reactive power minimization and current control for an indirect matrix converter under a distorted ac-supply," *IEEE Trans. Ind. Informat.*, vol. 8, no. 3, pp. 482–490, Aug. 2012.

[8] R. A. Mastromauro, M. Liserre, and A. Dell'Aquila, "Control issues in single-stage photovoltaic systems: MPPT, current and voltage control," *IEEE Trans. Ind. Informat.*, vol. 8, no. 2, pp. 241–254, Apr. 2012.

[9] A. Malinowski and Y. Hao, "Comparison of embedded system design for industrial applications," *IEEE Trans. Ind. Informat.*, vol. 7, no. 2, pp. 244–254, May 2011.

[10] M. P. Kazmierkowski, M. Jasinski, and G. Wrona, "DSP-based control of grid-connected power converters operating under grid distortions," *IEEE Trans. Ind. Informat.*, vol. 7, no. 2, pp. 204–211, May 2011.

[11] P. Tomei and C. M. Verrelli, "Observer-based speed tracking control for sensorless permanent magnet synchronous motors with unknown load torque," *IEEE Trans. Autom. Control*, vol. 56, no. 6, pp. 1484–1488, Jun. 2011.

[12] A. Piippo, M. Hinkkanen, and J. Luomi, "Analysis of an adaptive observer for sensorless control of interior permanent magnet synchronous motors," *IEEE Trans. Ind. Electron.*, vol. 55, no. 2, pp. 570–576, Feb. 2008.

[13] T. Orlowska-Kowalska and M. Dybkowski, "Stator-current-based MRAS estimator for a wide range speed-sensorless induction-motor drive," *IEEE Trans. Ind. Electron.*, vol. 57, no. 4, pp. 1296–1308, Apr. 2010.

[14] J. Kang, X. Zeng, Y. Wu, and D. Hu, "Study of position sensorless control of PMSM based on MRAS," in *Proc. IEEE Ind. Technol. Conf.*, Feb. 10–13, 2009, pp. 1–4.

[15] H. Abu-Rub, M. R. Khan, A. Iqbal, and S. M. Ahmed, "MRAS-based sensorless control of a five-phase induction motor drive with a predictive adaptive model," in *Proc. ISIE*, Jul. 4–7, 2010, pp. 3089–3094.

[16] J.-S. Jang, B.-G. Park, T.-S. Kim, D. M. Lee, and D.-S. Hyun, "Parallel reduced-order extended Kalman filter for PMSM sensorless drives," in *Proc. IEEE Ind. Electron. Soc. Annu. Conf.*, Nov. 2008, pp. 1326–1331.

[17] V. Smidl and Z. Peroutka, "Reduced-order square-root EKF for sensorless control of PMSM drives," in *Proc. IEEE Ind. Electron. Soc. Annu. Conf.*, Nov. 2011, pp. 2000–2005.

[18] D. Janiszewski, "Load torque estimation in sensorless PMSM drive using unscented Kalman filter," in *Proc. ISIE*, Jun. 27–30, 2011, pp. 643–648.

[19] Z. Q. Zhu and L. M. Gong, "Investigation of effectiveness of sensorless operation in carrier-signal-injection-based sensorless-control methods," *IEEE Trans. Ind. Electron.*, vol. 58, no. 8, pp. 3431–3439, Aug. 2011.

[20] G. Foo and M. F. Rahman, "Sensorless sliding-mode MTPA control of an IPM synchronous motor drive using a sliding-mode observer and HF signal injection," *IEEE Trans. Ind. Electron.*, vol. 57, no. 4, pp. 1270–1278, Apr. 2010.

[21] A. Accetta, M. Cirrincione, M. Pucci, and G. Vitale, "Sensorless control of PMSM fractional horsepower drives by signal injection and neural adaptive-band filtering," *IEEE Trans. Ind. Electron.*, vol. 59, no. 3, pp. 1355–1366, Mar. 2012.

[22] R. Leidhold, "Position sensorless control of PM synchronous motors based on zero-sequence carrier injection," *IEEE Trans. Ind. Electron.*, vol. 58, no. 12, pp. 5371–5379, Dec. 2011.

[23] G. Pellegrino, P. Giangrande, and L. Salvatore, "Sensorless position control of permanent-magnet motors with pulsating current injection and compensation of motor end effects," *IEEE Trans. Ind. Appl.*, vol. 47, no. 3, pp. 1371–1379, May/Jun. 2011.

[24] S. Bolognani, S. Calligaro, R. Petrella, and M. Tursini, "Sensorless control of IPM motors in the low-speed range and at standstill by HF injection and DFT processing," *IEEE Trans. Ind. Appl.*, vol. 47, no. 1, pp. 96–104, Jan./Feb. 2011.

[25] Y. Inoue, Y. Kawaguchi, S. Morimoto, and M. Sanada, "Performance improvement of sensorless IPMSM drives in a low-speed region using online parameter identification," *IEEE Trans. Ind. Appl.*, vol. 47, no. 2, pp. 798–804, Mar./Apr. 2011.

[26] J. B. Chu, Y. W. Hu, W. X. Huang, M. J. Wang, J. F. Yang, and Y. X. Shi, "An improved sliding mode observer for position sensorless vector control drive of PMSM," in *Proc. IEEE Power Electron. Motion Control Conf.*, May 2009, pp. 1898–1902.

[27] S. Chi, Z. Zhang, and L. Y. Xu, "Sliding mode sensorless control of direct drive PM synchronous motors for washing machine applications," *IEEE Trans. Ind. Appl.*, vol. 45, no. 2, pp. 582–590, Mar./Apr. 2009.

[28] K. C. Veluvolu and Y. C. Soh, "High-gain observers with sliding mode for state and unknown input estimations," *IEEE Trans. Ind. Electron.*, vol. 56, no. 9, pp. 3386–3393, Sep. 2009.

[29] Q. D. Nguyen and S. Ueno, "Improvement of sensorless speed control for nonsalient type axial gap self-bearing motor using sliding mode observer," in *Proc. IEEE Ind. Technol. Conf.*, Mar. 14–17, 2010, pp. 373–378.

[30] A. Jaafar, E. Godoy, P. Lefranc, X. Lin Shi, A. Fayaz, and N. Li, "Nonlinear sliding mode observer and control of high order dc–dc converters," in *Proc. IECON*, Nov. 7–10, 2010, pp. 180–186.

[31] H. Kim, J. Son, and L. Lee, "A high-speed sliding-mode observer for the sensorless speed control of a PMSM," *IEEE Trans. Ind. Electron.*, vol. 58, no. 9, pp. 4069–4077, Sep. 2011.

[32] A. Šabanovic, "Variable structure systems with sliding modes in motion control—A survey," *IEEE Trans. Ind. Informat.*, vol. 7, no. 2, pp. 212–223, May 2011.

[33] B. Wang and X. Li, "Computer-controlled variable structure systems: The state of the art," *IEEE Trans. Ind. Informat.*, vol. 8, no. 2, pp. 197–205, May 2012.

[34] X. Yu and O. Kaynak, "Sliding-mode control with soft computing: A survey," *IEEE Trans. Ind. Electron.*, vol. 56, no. 9, pp. 3275–3285, Sep. 2009.

[35] A. J. Mehta and B. Bandyopadhyay, "The design and implementation of output feedback based frequency shaped sliding mode controller for the smart structure," in *Proc. ISIE*, Jul. 4–7, 2010, pp. 353–358.

[36] G. Foo and M. F. Rahman, "Rotor position and speed estimation of a variable structure direct-torque-controlled IPM synchronous motor drive at very low speeds including standstill," *IEEE Trans. Ind. Electron.*, vol. 57, no. 11, pp. 3715–3723, Nov. 2010.

[37] Y.-S. Lu, "Sliding-mode controller design with internal model principle for systems subject to periodic signals," in *Proc. IEEE Amer. Control Conf.*, Jul. 2004, vol. 3, pp. 1952–1957.

[38] M. L. Corradini, G. Ippoliti, S. Longhi, and G. Orlando, "A quasi-sliding mode approach for robust control and speed estimation of PM synchronous motors," *IEEE Trans. Ind. Electron.*, vol. 59, no. 2, pp. 1096–1104, Feb. 2012.

[39] Z. Chen, M. Tomita, and S. Doki S, "New adaptive sliding observers for position and velocity sensorless controls of brushless dc motors," *IEEE Trans. Ind. Electron.*, vol. 47, no. 3, pp. 582–591, Jun. 2000.

[40] G. Tarchala, "Influence of the sign function approximation form on performance of the sliding-mode speed observer for induction motor drive," in *Proc. IEEE Int. Symp. Ind. Electron.*, 2011, pp. 1397–1402.

[41] G. L. Cascella, N. Salvatore, and L. Salvatore, "Adaptive sliding-mode observer for field oriented sensorless control of SPMSM," in *Proc. IEEE Ind. Appl. Conf.*, 2003, pp. 1137–1143.

[42] M. Comanescu, "Cascaded EMF and speed sliding mode observer for the nonsalient PMSM," in *Proc. IEEE Ind. Electron. Soc. Conf.*, Nov. 7–10, 2010, pp. 792–797.

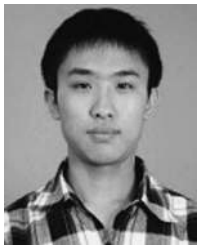

Zhaowei Qiao was born in Shanxi Province, China, in 1984. He received the B.S. degree from the Taiyuan University of Technology, Taiyuan, China, in 2007. He is currently working toward the Ph.D. degree in electrical engineering in the School of Electrical Engineering and Automation, Tianjin University, Tianjin, China.

His research interests include wind power technology, power electronics, motor design, and motor drivers.

Tingna Shi was born in Zhejiang, China, in 1969. She received the B.S. and M.S. degrees from Zhejiang University, Hangzhou, China, in 1991 and 1996, respectively, and the Ph.D. degree from Tianjin University, Tianjin, China, in 2008.

She is currently an Associate Professor with the School of Electrical Engineering and Automation, Tianjin University. Her research interests include electrical machines and their control systems, power electronics, and electric drives.

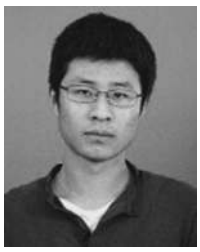

Yindong Wang was born in Jilin, China, in 1986. He received the M.S. degree in control science and engineering from Tianjin University, Tianjin, China, in 2011.

His major field of study included electrical drives and industrial automation instrument. He is currently a Researcher with Tianjin Aviation Electro-Mechanical Company, Ltd., Tianjin. His current research areas include power electronics and switching power supply.

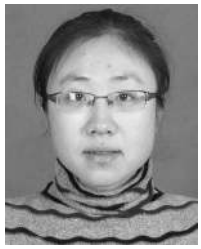

Yan Yan was born in Tianjin, China, in 1981. She received the B.S. and M.S. degrees in electrical engineering from the Tianjin University of Science and Technology, Tianjin, in 2004 and 2007, respectively, and the Ph.D. degree in electrical engineering from Tianjin University, Tianjin, in 2010.

She is currently a Lecturer with the School of Electrical Engineering and Automation, Tianjin University. Her research interests include the design and control of matrix converter for electric drive applications and power converters for wind power generation.

Changliang Xia (M'08–SM'12) was born in Tianjin, China, in 1968. He received the B.S. degree in electrical engineering from Tianjin University, Tianjin, in 1990 and the M.S. and Ph.D. degrees in electrical engineering from Zhejiang University, Hangzhou, China, in 1993 and 1995, respectively.

He is currently a Professor in the School of Electrical Engineering and Automation, Tianjin University, and also in the Tianjin Key Laboratory of Advanced Technology of Electrical Engineering and Energy, Tianjin Polytechnic University, Tianjin. In 2008, he became "Yangtze Fund Scholar" Distinguished Professor and is currently supported by the National Science Fund for Distinguished Young Scholars. His research interests include electrical machines and their control systems, power electronics, and control of wind generators.

Xiangning He (M'95–SM'96–F'10) received the B.Sc. and M.Sc. degrees from the Nanjing University of Aeronautics and Astronautics, Nanjing, China, in 1982 and 1985, respectively, and the Ph.D. degree from Zhejiang University, Hangzhou, China, in 1989.

From 1985 to 1986, he was an Assistant Engineer with the 608 Institute of Aeronautical Industrial General Company, Zhuzhou, China. From 1989 to 1991, he was a Lecturer with Zhejiang University. In 1991, he received a Fellowship from the Royal Society of U.K. and conducted research in the Department of Computing and Electrical Engineering, Heriot-Watt University, Edinburgh, U.K., as a Postdoctoral Research Fellow for two years. In 1994, he joined Zhejiang University as an Associate Professor, where he has been a Full Professor since 1996. He is currently the Vice Dean of the College of Electrical Engineering, Zhejiang University. His research interests include power electronics and their industrial applications.